

Enhanced Osteogenic Behavior of ADSCs Produced by Deproteinized Antler Cancellous Bone and Evidence for Involvement of ERK Signaling Pathway

Jinqi Wei,^{1,2,*} Mingming Xu,^{1,*} Xuehui Zhang,^{1,3} Song Meng,¹ Yixiang Wang,⁴ Tuanfeng Zhou,² Qi Ma,¹ Bing Han,⁵ Yan Wei,¹ and Xuliang Deng^{1,6}

Calcinated antler cancellous bone (CACB) is useful in repair of bone defects, as its composition and architecture is analogous to natural extracellular bone matrix. The use of CACB scaffolds with adipose-derived stem cells (ADSCs) in repair of rabbit mandibular bone defects was investigated along with the underlying molecular signaling pathways involved. CACB promoted the adhesion, spreading, and viability of ADSCs. Increased extracellular matrix production and expression of osteogenic markers in ADSCs were observed when seeded in CACB. The temporal kinetics of mRNA expression of ADSCs cultured in CACB lagged in comparison with that observed in cells grown in medium with osteogenic supplements. Activation of the extracellular signal-related kinases (ERK) 1/2 and RUNX-2 in CACB-cultured ADSCs was observed, and this activation was attenuated by the MeK inhibitor U0126. Microcomputed tomography scanning analysis and histological evaluations showed that loading the CACB with ADSCs resulted in enhanced new bone formation and angiogenesis when the composites were implanted in rabbit mandibular defects. These results indicated that the osteogenic behavior of ADSCs might be driven by the microenvironment formed by CACB via the ERK signaling pathway. These CACB/ADSCs composites have promising therapeutic potential for large bone defect repairs.

Introduction

IN ORTHOPEDICS, ORAL AND MAXILLOFACIAL surgery repairing large bone defects with predictable results is still a substantial challenge. The use of autografts remains the “gold standard” technique for bone defect repair, despite the disadvantages of donor site morbidity and limited availability.^{1,2} Using allogenic bone grafts is an alternative, but this technique has the disadvantages of possible disease transmission, immune reaction, and uncertain healing outcomes.^{3–5} Xenogenic bone grafts are promising candidate grafts as they have excellent osteoconductivity, biosecurity and are easily accessible.⁶ However, the clinical outcome is not always satisfactory due to the lack of functional cells and bioactive growth factors.⁷

Using xenografts combined with seed cells, to mimic the osteogenic niche provided by autografts, has become popular in the past few decades.^{8–13} In theory, progenitor cells or stem cells seeded into grafts are thought to be affected by

the microenvironment formed by the xenografts, will give rise to a hierarchy of bone-forming cell populations, and serve as a source of growth factors to advance the healing process.¹⁴ The outcome appears to be determined by how the microenvironments formed by the physiochemical properties of xenografts affect the bioactivity and differentiation of the seed cells.^{14,15} Hence, an understanding of the responses of seed cells to xenogenic grafts and of the underlying mechanisms is fundamental, which may provide the basis not only for modifying the efficiency and kinetics of bio-engineered bone regeneration but also for promoting their clinical application.

Numerous commercially available inorganic xenograft bone substitutes such as Bio-Oss[®], Endobon[®], and Osteo-Biol[®] have been used in clinics. The efficacy of the combination of xenografts with mesenchymal stem cells (MSCs) or osteoblast progenitor cells in the repair of bone defects has been tested. Bareille *et al.* demonstrated an early formation of lamellar bone when Endobon/human bone

¹Department of Geriatric Dentistry, Peking University School and Hospital of Stomatology, Beijing, People's Republic of China.

²First Clinical Division, Peking University School and Hospital of Stomatology, Beijing, People's Republic of China.

³Department of Dental Materials, Peking University School and Hospital of Stomatology, Beijing, People's Republic of China.

⁴Central Laboratory, Peking University School and Hospital of Stomatology, Beijing, People's Republic of China.

⁵Department of Orthodontics, Peking University School and Hospital of Stomatology, Beijing, People's Republic of China.

⁶National Engineering Laboratory for Digital and Material Technology of Stomatology, Peking University School and Hospital of Stomatology, Beijing, People's Republic of China.

*These authors contributed equally to this work.

marrow stromal cell (BMSCs) composites were implanted subcutaneously in euthymic mice.¹¹ Similar results have been obtained with Bio-Oss combined with BMSCs in sinus augmentations in adult sheep.¹² Although it has been demonstrated that xenograft bone substitutes can act as optimized carriers of MSCs/progenitor cells and may have favorable clinical therapeutic efficacies, the disadvantages of their time-consuming manufacturing process and the controversial ethical issues of animal welfare are likely to impede their clinical application. In previous studies, we proposed calcinated antler cancellous bone (CACB) as a new source of inorganic xenogenic bone substitute, as it has the advantages of good reproducibility and easy accessibility and is acceptable in terms of animal welfare and ethical considerations.^{16,17} Due to its close similarities to human cancellous bone in mineral composition, physical properties, and interconnecting pore structures, CACB has potential for utilization in bone defect repairs.¹⁶ Its compatibility with bioactive molecules of different molecular weight and sources has also been studied.¹⁷ However, the effects of the microenvironment formed by the physiochemical properties of CACB on directing osteogenic differentiation of MSCs or osteoblast progenitor cells remain unknown.

Adipose-derived stem cells (ADSCs) are proved to have multilineage capability and gain extensive attention for their large amount with simple, inexpensive, and less invasive harvesting procedures.^{18–20} ADSCs have also exhibited promising bone defect repair efficacies not only in animal studies^{8,13,14,21} but also in clinical application when combined with fibrin and ceramics.^{22–24} However, the temporal kinetics and mechanisms underlying the osteogenic behavior of ADSCs in the

xenogenic bone substitute remains unknown. An understanding of the biological processes and mechanisms of the osteogenic activity of ADSCs produced by CACB bone grafts is necessary to hone this technique for clinical use.

This study explores the osteogenic behavior of ADSCs produced by CACB and investigates the biocompatibility of ADSCs with CACB in terms of adhesion, proliferation, and extracellular matrix secretion. The expression of osteogenic marker genes mediated by the microenvironment of CACB was examined, and the possible involvement of the extracellular signal-related kinase (ERK) signaling pathway was investigated. The efficacy of the CACB/ADSCs composites in rabbit mandible defect repair was explored to confirm their clinical potential.

Materials and Methods

Characterization of CACB scaffolds

The CACB scaffolds were prepared as previously reported.¹⁶ Briefly, the cancellous portion of the antler was cut into cubes sized $6 \times 5 \times 2$ mm. The cubes were immersed in 2 M sodium hydroxide solution for 24 h, then in a 3:1 mixture of chloroform and methanol for 1 h, and then in 30% hydrogen peroxide for 24 h. After each step, the cubes were twice washed with distilled water. Finally, the cubes were dried at 70°C for 24 h and then sintered at 800°C for 6 h in a tube-type furnace to obtain CACB (Fig. 1A). The interconnected pore structure of the scaffold was examined using microcomputed tomography scanning (μ -CT) with a Skyscan 1172 system (Skyscan NV). The surface morphology and structure were observed using scanning electron microscopy

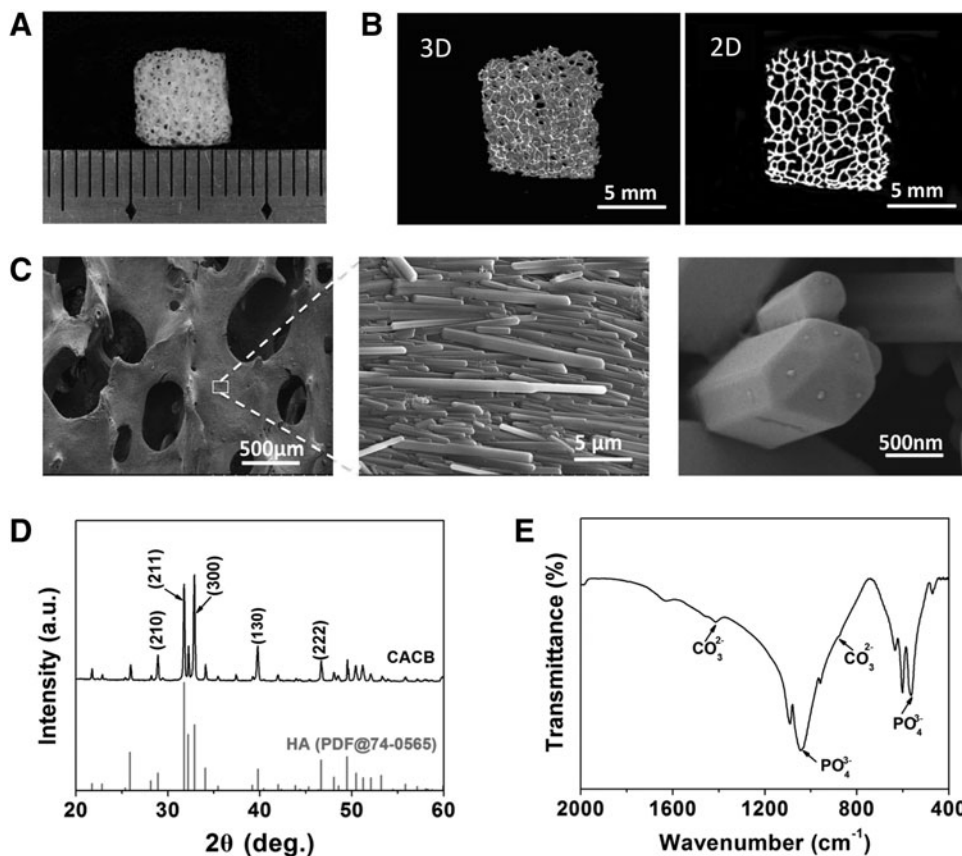


FIG. 1. Morphology, crystalline phase, and chemical composition of calcinated antler cancellous bone (CACB). (A) The macroscopic images, (B) micro-computed tomography (μ -CT) images of three-dimensional (3D) and two-dimensional (2D) reconstruction of the CACB cube. (C) Scanning electron microscopy (SEM) images of the macro-porous structure and hydroxyapatite (HA) crystal morphology of CACB. (D) X-ray diffraction spectroscopy (XRD) patterns and (E) Fourier transform infrared spectroscopy (FTIR) spectroscopy of CACB scaffolds.

(SEM; ZEISS, Supra 55) after the samples were sputter coated with gold at a voltage of 15.0 kV.

The phase composition of CACB was analyzed using powder X-ray diffraction spectroscopy (XRD; D/max 2500 VB2 +/PC; Rigaku). Fourier transform infrared spectroscopy (FTIR; Avatar 360; Nicolet Co.) was used to evaluate the infrared absorption spectra of CACB in the 4,000–400 cm^{-1} range.

Isolation, expansion of rabbit ADSCs

Twelve male New Zealand White rabbits (Center of Experimental Animal, Peking University School and Hospital of Stomatology) with each weighing ~ 1.5 kg per one were used. The experimental protocol was approved by the Animal Care and Use Committee of Peking University. ADSCs from each rabbit (RaADSCs) were isolated as previously reported.¹³

Observation of cell morphology on CACB

A 200 μL aliquot of the RaADSC cell suspension at a concentration of 2×10^6 cells/mL was added into each scaffold in a 24-well plate (Corning, Inc.). After 1 and 7 days of culture in the common medium (10% fetal bovine serum in Dulbecco's modified Eagle's medium, containing 1% penicillin/streptomycin; Cyagen Biosciences, Inc.), the RaADSCs in CACB were fixed with 2.5% glutaraldehyde, afterward immersed in a 0.18 M saccharose solution for 2 h, and then dehydrated using an increasing ethanol gradient. The samples were dried overnight, sputter-coated with gold, and observed using SEM at 15 kV.

Cell proliferation analysis

After being cultured for 1, 3, or 7 days, samples were fixed with 3.7% paraformaldehyde. The F-actin filaments were stained with 50 $\mu\text{g}/\text{mL}$ rhodamine phalloidin (Sigma-Aldrich). The nuclei were stained using 0.3 μM 4', 6-diamidino-2-phenylindole (DAPI; Sigma-Aldrich). The samples were observed using Confocal Laser Scanning Microscopy (CLSM; Carl Zeiss). Five visual fields were randomly captured for each sample, and cells were numbered by nuclei counting. Three separate experiments were performed. At 1, 3, 5, and 7 days after seeding, the DNA content was measured using Quant-iT™ dsDNA HS Assay Kit (Invitrogen) according to the manufacturer's instructions.

Immunofluorescence staining

Four groups were used in this experiment: the CACB/OS– group, RaADSCs seeded in CACB and cultured in common medium; the CACB/OS+ group, RaADSCs seeded in CACB and cultured in osteoinductive medium (OS, common medium containing 10 nmol/L dexamethasone, 20 mmol/L β -glycerophosphate, 0.05 mmol/L ascorbic acid); the TCPs/OS– group, cells cultured in tissue culture plates (TCPs) with common medium; and the TCPs/OS+ group, cells cultured in TCPs with osteoinductive medium. After culturing for 7 and 14 days, cell samples were fixed in 3.7% paraformaldehyde. Subsequently, the cells were permeabilized with 0.1% Triton X-100/phosphate-buffered saline for 5 min, blocked with 3% bovine serum albumin, and then incubated with a 1:500 dilution of the primary antibodies to collagen type I (Col I), osteocalcin (OCN; Abcam, Inc.) or osteopontin (OPN; custom made from Abcam, Inc.) overnight at 4°C. Afterward, the cells were incubated with a 1:250 dilution of the secondary antibody (FITC-conjugated Affinipure goat anti-mouse IgG; Abcam, Inc.). Finally, cell nuclei were stained with DAPI. The samples were observed using CLSM. The staining intensities of Col I, OCN, and OPN were analyzed by Image Pro Plus Software (Media Cybernetics).

Real-time quantitative PCR analysis

After 7, 14, and 21 days of culture, cells were lysed with Trizol Reagent (Ambion) and total RNA was extracted according to the manufacturer's instructions. First-strand cDNA was synthesized with the ReverTra Ace qPCR RT Master Mix (Toyobo Co., Ltd.). Real-time quantitative polymerase chain reaction (RT-qPCR) using Fast-Start Universal SYBY Green Master (Rox; Roche Ltd.) was performed using a 7500 Real-Time PCR System (Life Technologies, Inc.). Relative quantification was carried out using the $\Delta\Delta\text{Ct}$ method. Three separate experiments were performed. The sequences of gene primers used for RT-qPCR are listed in Table 1.

Western blot analysis

On the third day after seeding, total cellular protein was extracted as previously described.¹⁴ Briefly, cells were lysed with ice-cold RIPA (Thermo Fisher Scientific) containing phosphatase inhibitor cocktail (Applygen). For each sample, 25 μg of protein was resolved on sodium dodecyl sulfate

TABLE 1. PRIMERS USED FOR RT-qPCR

Gene		Sequence (5'-3')	No.
ALP	Forward	TCAGCTTCCTCCTCTTTGCG	XM_002716044.1
	Reverse	CGGGTCCACAGTTCAGGAAA	
BMP2	Forward	ACTGCCAGAAACAAGTGGGA	NM_001082650.1
	Reverse	TGATGGAAACCGCTGTCGTC	
OPN	Forward	TGGCTAAACCCTGACCCAT	NM_001082194.1
	Reverse	TATCCACGTGGTCATCGTCC	
BSP	Forward	ACGCTTTCTTTTACAACACCTG	XM_002717020.1
	Reverse	GCTGGTGCCATTGATGCTCTG	
GAPDH	Forward	GTATGATTCCACCCACGGCA	NM_001082253.1
	Reverse	CCAGCATCACCCCACTTGAT	

RT-qPCR, real-time quantitative polymerase chain reaction.

polyacrylamide gels and electrotransferred onto PVDF membranes (Millipore Corporation). The membranes were blotted using 5% Carnation nonfat dry milk and incubated with anti-p-ERK antibody, anti-ERK antibody, anti-RUNX-2 antibody, and anti-GAPDH antibody (custom made from Abcam, Inc.) overnight at 4°C, respectively. Then, the primary antibodies were detected using horseradish peroxidase (HRP)-conjugated secondary antibodies. To verify the role of the ERK1/2 signaling pathway in the osteogenic differentiation of RaADSCs mediated by CACB, the selective inhibitor U0126 (Cell Signaling Technology, Inc.) was used at a final concentration of 20 µM. The protein bands were visualized using the ECL chemiluminescence reagent (Thermo Fisher Scientific) and were quantified using an image analysis system (Quantity One software; Bio-Rad).

In vivo osteogenesis of CACB combined with ADSCs

Preparation of implantation composites. About 1.5×10^6 cells of the third passage from each rabbit were seeded on 0.25 mg CACB, which had been ground into particles of ~1.0–2.0 mm in diameter, and then cultured for 7 days in preparation for the *in vivo* study.

Surgical procedures. Bone defects in each side of the mandibles of 12 rabbits were created as described in our previous report¹⁶ and were randomly divided into three groups: (1) CACB group: eight defects for implantation with 0.25 mg CACB granules; (2) CACB/ADSCs group: eight defects for implantation with CACB seeded with ADSCs; and (3) Untreated group: eight defects were left untreated as controls. Rabbits from each group were sacrificed using lethal intravenous administrations of sodium pentobarbital at 4 and 12 weeks postimplantation.

µ-CT analysis. At 12 weeks postimplantation, the mandibles were harvested intact and fixed in 4% paraformaldehyde, and the specimens were examined using µ-CT scanning. Files were reconstructed using a modified Feldkamp algorithm, which was created using µ-tomographic analysis software (Tomo NT; Skyscan). After three-dimensional (3D) visualization, bone morphometric analyses, including bone coverage, bone density, and bone volume in the bone defects, were carried out on the region of interest.

Histological and immunohistochemical examinations. Four and 12 weeks postsurgery, all rabbit mandibles from all three groups were subjected to tissue processing and sectioning. The samples were fixed in 10% formalin for 24 h and demineralized in 15% formic acid for 6 weeks. The tissues were then embedded in paraffin and sectioned to a 4 µm thickness. Hematoxylin and eosin staining was performed on tissue sections according to the manufacturer's protocols. The images were captured using light microscopy (CX21; Olympus). The amount of new bone and bone marrow cavities was analyzed by Image Pro Plus Software (Media Cybernetics).

The number of blood vessels at the implantation site was determined by immunohistochemical analysis. De-paraffinized sections were washed, and nonspecific endogenous peroxidase activity was quenched by immersing in 3% H₂O₂/methanol for 15 min, then incubated with anti-CD31 primary

antibody (1:200; Abcam) for 2 h. HRP-conjugated secondary antibody was applied to the slides for 1 h at room temperature. Finally, the diaminobenzidine (DAB; Beyotime) kit was used to develop the color, followed by counterstaining with hematoxylin. A vascular section was defined as a vessel with a recognizable lumen. Micro hemorrhages were excluded in the vessel count. Three different individuals performed the evaluation with single blind.

Statistical analysis

All quantitative data are expressed as mean ± standard error. Statistical analyses were performed using SPSS 13.0 software. The Shapiro–Wilk test was applied to check whether the values were normally distributed. One-way ANOVA and *post hoc* multiple comparison tests were used to analyze the differences of the results of the immunofluorescence staining, the RT-qPCR, and the western blotting, and they were also used to analyze the differences in bone coverage, bone density and bone volume, the amount of new bone, bone marrow cavities, and blood vessel sections in the animal experiments. When the variances among different groups were not equal, Dunnett T3 test was applied to evaluate the differences. Differences between groups where * $p < 0.05$ were considered statistically significant and where ** $p < 0.01$, the differences were considered highly significant.

Results

Characterization of the CACB

The highly porous structures of the CACB are shown in both SEM images, and the two-dimensional and 3D reconstructed µ-CT images (Fig. 1A–C). The well-interconnected macropores range in size from ~300–700 µm. The basic elements of the CACB are six-sided prismatic hydroxyapatite (HA) crystals that are 400–600 nm wide and 5–15 µm long (Fig. 1C). The phase composition of CACB is demonstrated by the XRD spectrum (Fig. 1D). CACB is mainly composed of highly crystallized HA with small amounts of other chemicals such as carbonate HA and Mg₂P₄O₁₂·8H₂O. The FTIR spectra show the presence of phosphate (PO₄³⁻), hydroxyl (OH⁻), and carbonate (CO₃²⁻) ions in the CACB (Fig. 1E).

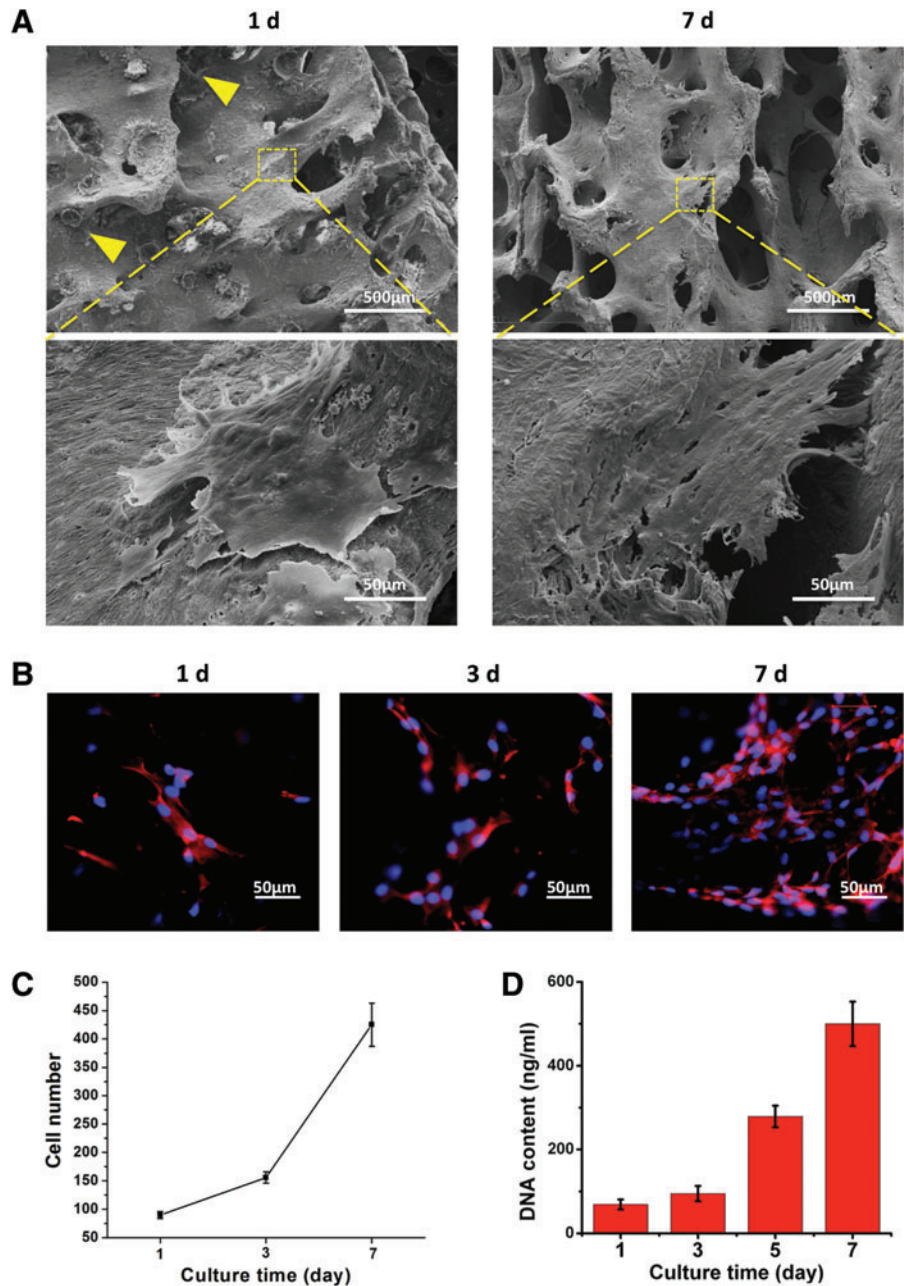
Cell adhesion and proliferation of ADSCs on CACB

Fig. 2A shows the cell adhesion and morphologies of RaADSCs in CACB scaffolds. Highly branched ADSCs with pseudopodia spreading on the surface of the CACB were observed 1 day after seeding. After 7 days of cultivation, dense lamellipodia stretched out from the RaADSCs to cover the trabeculae and span the pores. Cell proliferation in CACB scaffolds after 1, 3, and 7 days was observed using CLSM (Fig. 2B). The cell number and DNA content of RaADSCs in CACB increased with prolonged incubation time (Fig. 2C, D). The growth of RaADSCs entered the logarithmic growth phase on the third day.

Osteogenic differentiation of ADSCs in CACB

Immunofluorescence staining of Col I, OCN, and OPN in RaADSCs is shown in Figure 3. On day 7, CACB promoted the secretion of Col I and OCN in the RaADSCs with or without OS induction (Fig. 3A). Qualitatively, both the

FIG. 2. Cell adhesion and proliferation in CACB. **(A)** Cell adhesion and morphologies of RaADSCs in CACB scaffolds after 1 and 7 days of incubation, observed by SEM. *Yellow arrow heads* denote the well-attached RaADSCs in CACB. The lower images are enlargements of specific regions in the corresponding upper ones. **(B)** Cell proliferation of RaADSCs in CACB scaffolds after 1, 3, and 7 days observed by confocal laser scanning microscopy (CLSM). Cells were stained with rhodamine phalloidin (cytoskeleton, *red*) and 6-diamidino-2-phenylindole (DAPI) (nuclei, *blue*). **(C)** The growth curve of RaADSCs in CACB scaffolds over 7 days. **(D)** The DNA content of RaADSCs in CACB scaffolds after 1, 3, 5, and 7 days. RaADSCs, rabbit adipose-derived stem cells. Color images available online at www.liebertpub.com/tea



CACB/OS⁻ group and TCPs/OS⁺ group had similar staining intensities (Fig. 3C). No visible OPN staining was detected in any group.

After 14 days, the production of Col I, OCN, and OPN were significantly increased in all the groups compared with that on day 7 (Fig. 3B). On day 14, both the CACB/OS⁻ and TCPs/OS⁺ groups showed similar intensities (Fig. 3C).

The temporal kinetics of the mRNA expression of *ALP*, *BMP2*, *OPN*, and *BSP* in cultured ADSCs on day 7, 14, and 21 are shown in Fig. 4. CACB increased the expression of all selected osteogenic marker genes, and higher expression levels were achieved at all experimental time points when CACB was combined with OS. At day 7, the expression levels of *ALP*, *BMP2*, *BSP*, and *OPN* were higher in the TCPs/OS⁺ group than those in the CACB/OS⁻ group ($p < 0.05$) (Fig. 4A). However, between 7 and 14 days, the

expression levels of these osteogenic marker genes in the CACB/OS⁻ group increased rapidly to reach similar levels with those in the TCPs/OS⁺ group ($p > 0.05$) (Fig. 4B). After 21 days, the expression levels of *OPN* in the CACB/OS⁻ group were much higher than those in the TCPs/OS⁺ group ($p < 0.05$) (Fig. 4C).

ERK pathway analysis

As depicted in Fig. 5, in comparison to the TCPs group, CACB initiated a significant increase in the ratio of phosphorylated ERK1/2 (P-ERK1/2)/ERK1/2, suggesting the activation of the ERK pathway. The expression of the downstream osteogenic marker RUNX-2 was correspondingly enhanced. When the MeK1/2 inhibitor U0126 was added, decreased level of P-ERK1/2 in the ADSCs in CACB

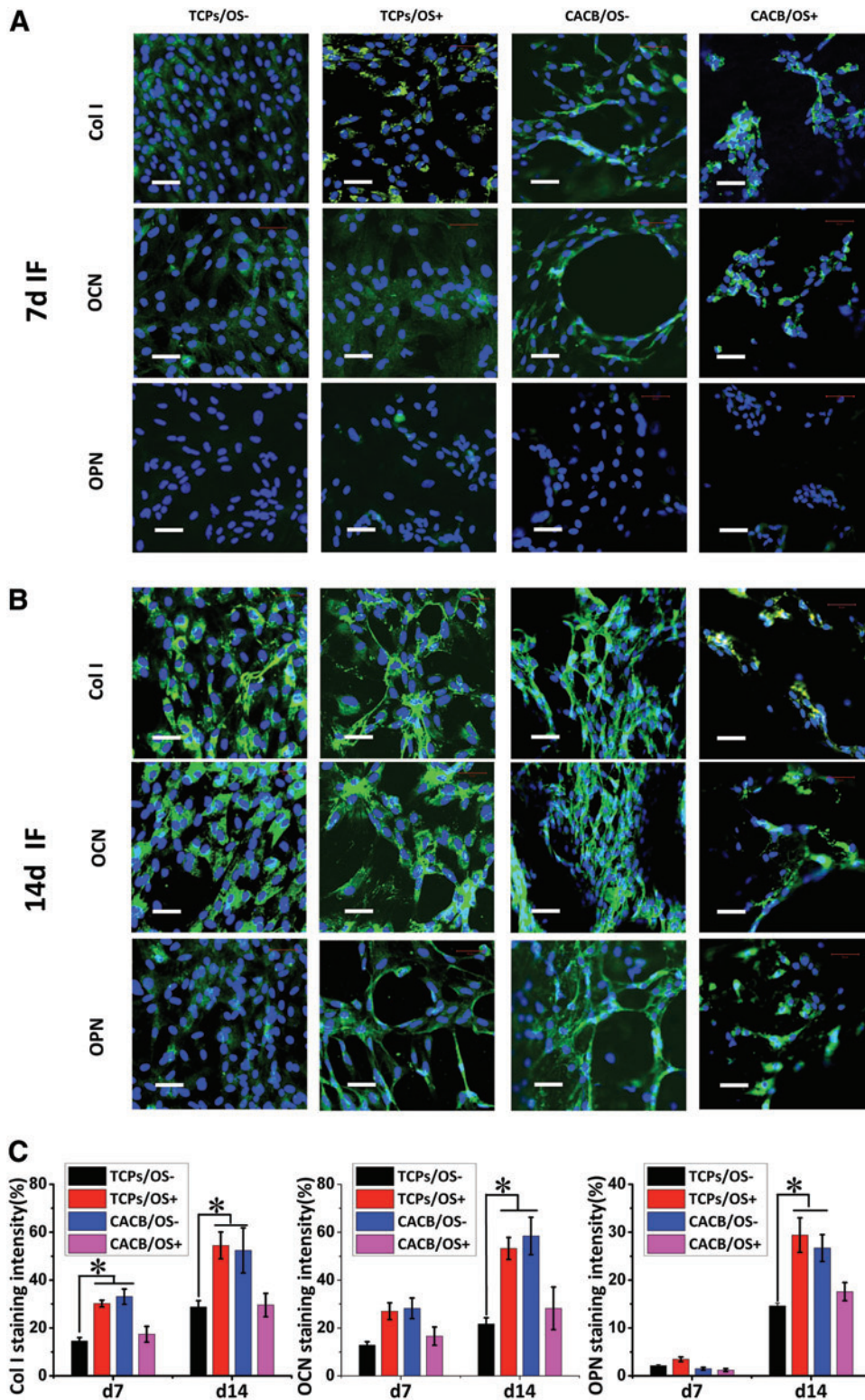


FIG. 3. Immunofluorescence staining (IF) of collagen type I (Col I), osteocalcin (OCN), and osteopontin (OPN) in RaADSCs cultured for 7 (A) and 14 days (B). (C) Semi-quantitative analysis of relative expression levels of Col I, OCN, and OPN. Scale bar = 50 μ m. Color images available online at www.liebertpub.com/tea

was demonstrated, which was accompanied by an apparent decreased expression of RUNX-2.

Repair of rabbit mandible bone defects

Representative 3D morphological μ -CT scanning images of repaired rabbit mandible defects are shown in Figure 6. In

the untreated group, the mandibular defect was left with an obvious introcession (Fig. 6A). At 12 weeks, substantial new bone formation was observed in both the CACB and the CACB/ADSCs groups (Fig. 6A). Qualitatively, the surface morphology of the healing area in the CACB/ADSCs group more closely resembles the surrounding normal bone tissue than that in the CACB group. The morphometric analyses of

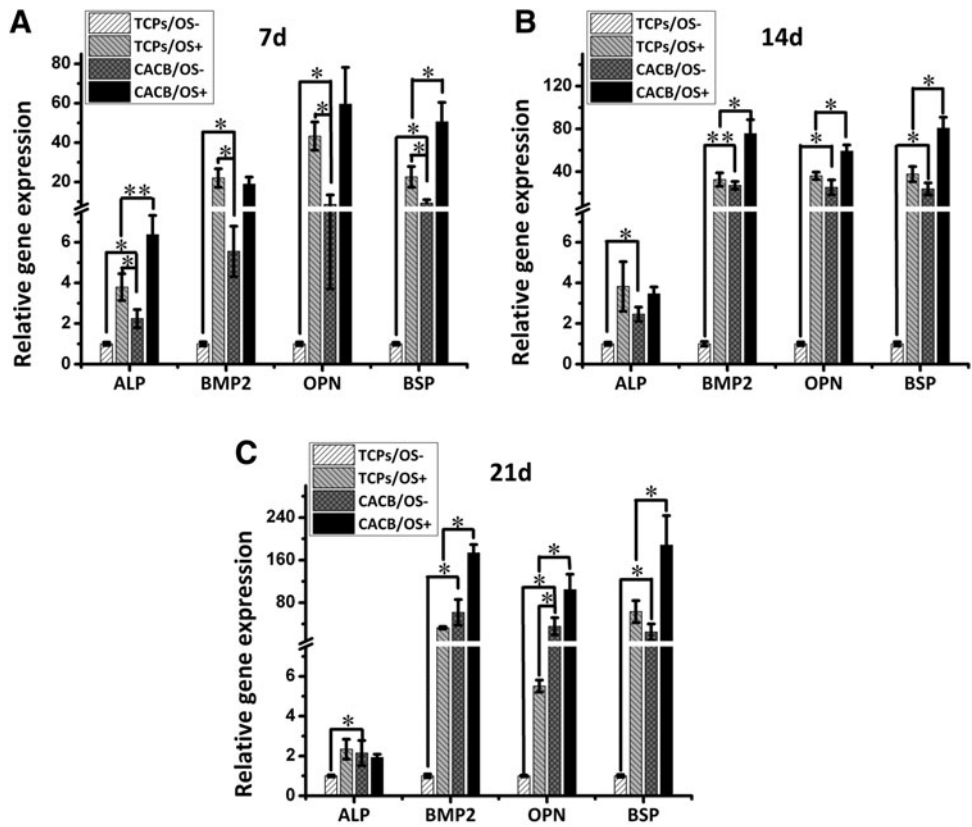


FIG. 4. Gene expression profiles of *ALP*, *BMP2*, *OPN*, and *BSP* analyzed by real-time quantitative polymerase chain reaction (RT-qPCR) after 7 (A), 14 (B) and 21 days (C) of incubation. Cells cultured in TCPs/OS- were used as the control group. * $p < 0.05$ and ** $p < 0.01$.

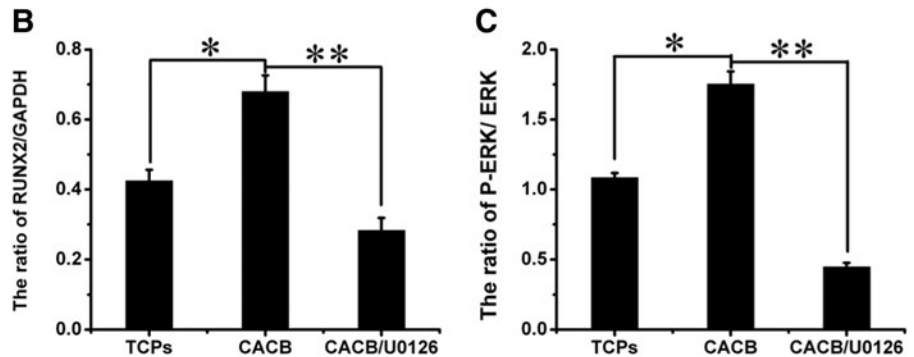
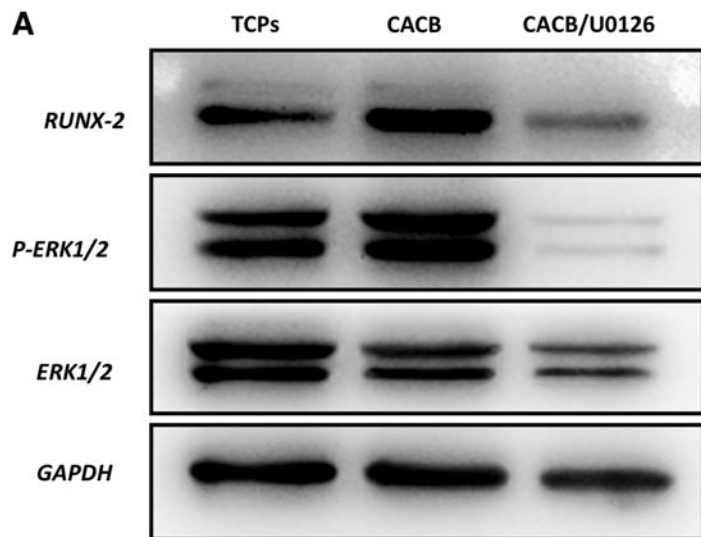


FIG. 5. (A) Activation of extracellular signal-related kinase (ERK) pathway proteins in RaADSCs observed by western blot analysis. (B) Semiquantitative the amount of RUNX-2 and (C) comparison of the ratio of P-ERK/ERK among TCPs, CACB and CACB/U0126 groups. * $p < 0.05$, ** $p < 0.01$.

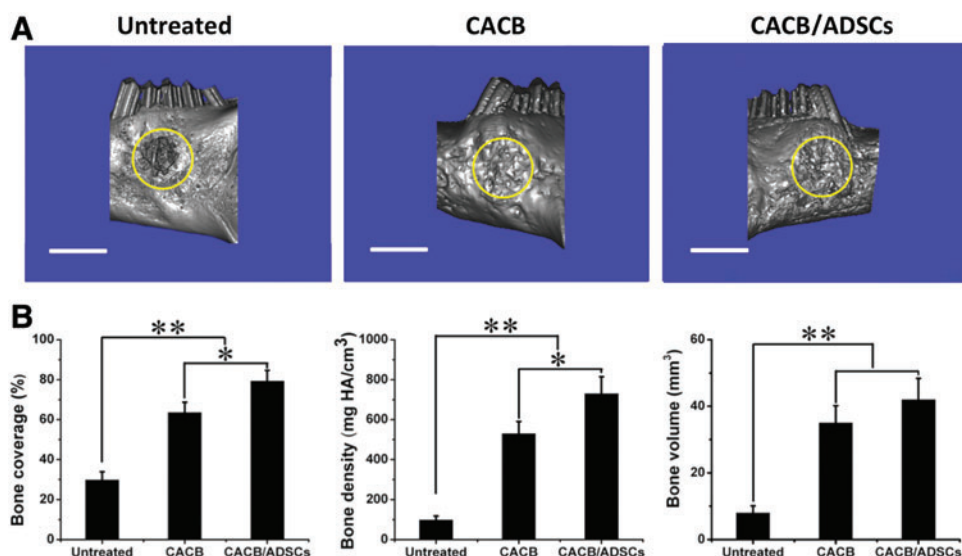


FIG. 6. (A) Representative 3D μ -CT images of rabbit mandibular bone defects in untreated group, CACB group, and CACB/adipose-derived stem cells (ADSCs) group. (B) Quantitative analysis of bone coverage, bone density, and bone volume at 12 weeks post-implantation. Scale bar = 8 mm. Yellow circles denote the surgical site. * $p < 0.05$ and ** $p < 0.01$. Color images available online at www.liebertpub.com/tea

newly formed bone quantity in the defect sites demonstrated that higher values of bone coverage, bone density, and bone volume were achieved by the CACB/ADSCs than by CACB alone (Fig. 6B).

As shown in Figure 7, at 4 weeks postimplantation, fat vacuoles were observed as filling in the defect area in the untreated group (Fig. 7A). A small amount of new bone was found in the CACB group defects, while significantly increased amounts of new bone were observed in the CACB/ADSCs group ($p < 0.05$) (Fig. 7A, D). At 12 weeks post-implantation, there was still little new bone found in the untreated defects (Fig. 7B). The CACB/ADSCs implantation resulted in the formation of mature, regular bony trabeculae, while fewer, immature trabeculae were found in the CACB group ($p < 0.05$) (Fig. 7B, D). CD31 staining showed significantly more new vessels in the CACB/ADSCs group than those in the CACB group at both time points of 4 and 12 weeks ($p < 0.05$) (Fig. 7C, D).

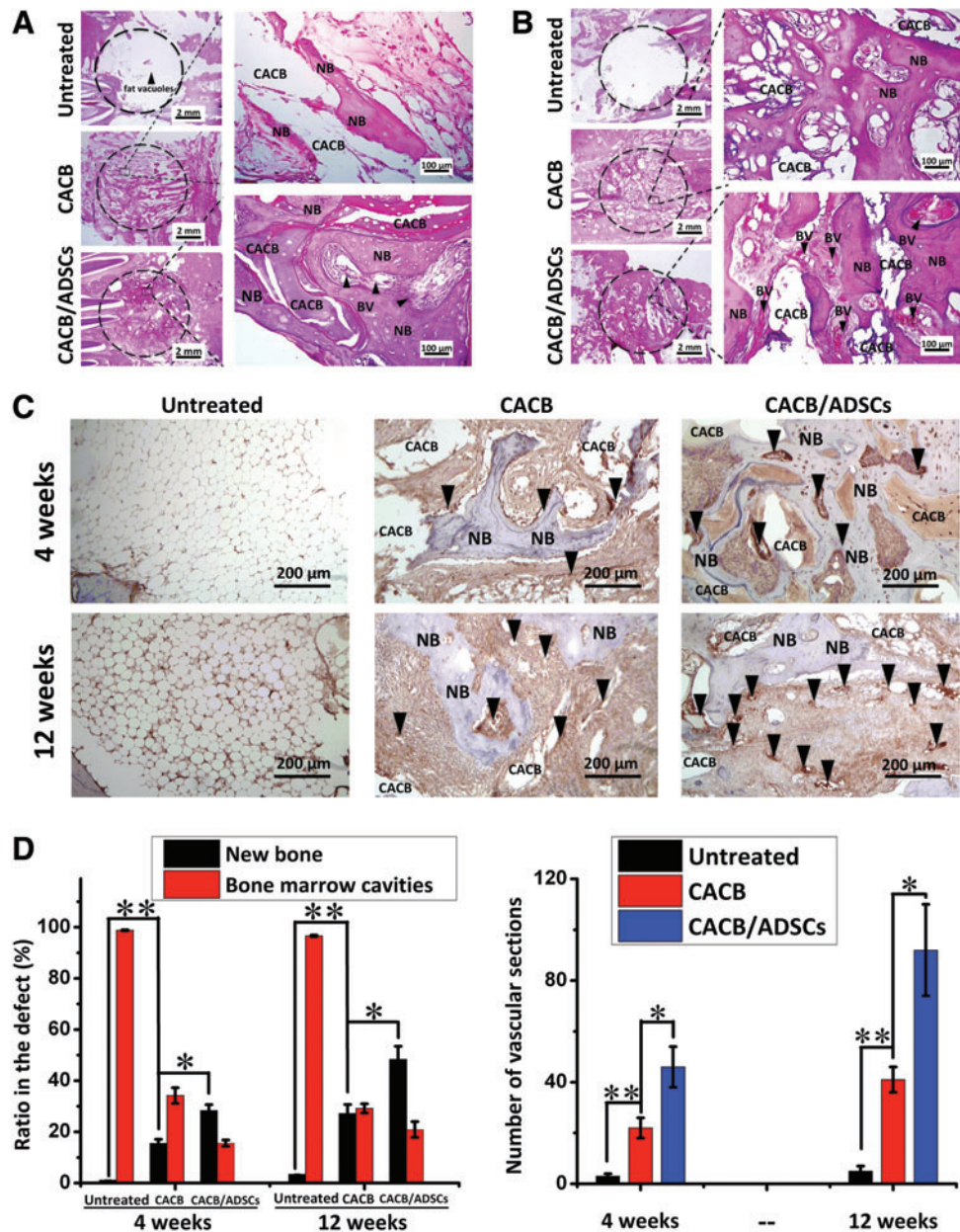
Discussion

The microenvironmental cues created by the physiochemical characteristics of bone graft substitutes exert a considerable influence on the function and differentiation of MSCs.^{25–28} As a xenogenic bone graft, CACB maintains most of its physiological inorganic composition and architecture analogous to the bone extracellular matrix. Its use would avoid the controversial ethical and animal welfare issues of xenogenic grafts.^{16,17} ADSCs have multiple differentiation capability, easy accessibility, and reduced donor morbidity and are promising seed cells for positive osteogenesis.^{18,19} To provide a strategy combining ADSCs and CACB for clinical regenerative therapies, it is required to clarify the maintenance of bioactivity and the differentiation modulation of ADSCs in CACB, and their synergistic effects in the bone-healing process. We have demonstrated that CACB could provide an appropriate microenvironment to produce osteogenic differentiation of ADSCs via the ERK signaling pathway. CACB/ADSCs composites have shown therapeutic potential in the repair of large bone defects.

Our results indicated that the multi-scale topography and biomimetic chemical niche provided by CACB improved ADSC viability and promoted the cells to extend dense lamellipodia and filopodia to establish close cell-material connections. Such biocompatibility between scaffolds and cells is important for the bone defect healing process. Muller *et al.* and Cui *et al.* have reported that bovine-derived xenogenic bone grafts provide a natural architectural matrix to allow the integration of host cells and increase the available surface area to improve cell adhesion.^{21,26} In our previous studies, antler-derived CACB favored cell spreading and proliferation of BMSCs *in vitro*,¹⁷ consistent with the biocompatibility between CACB and ADSCs observed in this work. The six-sided prismatic nano-scale-sized HA crystals of the CACB could provide multiple binding sites for the amino and carboxyl groups of serum proteins, which, in turn, could facilitate cell attachment²⁹ and bone matrix deposition,³⁰ consequently enhancing the function and differentiation of MSCs. Furthermore, the chemical components of CACB, HA^{31,32} and trace amounts of Si^{31,33–35} and Zn ions,^{36,37} can accelerate cell adhesion and proliferation by delivering mitogenic stimuli and enhancing channel sensitivity.

In our study, the CACB was used to drive ADSCs down the osteogenic lineage without using osteogenic supplements. There are controversial opinions regarding whether the xenogenic grafts possess the capability of promoting osteogenic differentiation. Acil *et al.*³⁸ and Cui *et al.*²¹ reported that xenogenic grafts lacked the capability of enhancing osteogenic lineage. However, some results indicated that xenogenic grafts could promote osteogenic differentiation of stromal cells. Kubler *et al.* demonstrated lower ALP activities in human osteoblasts seeded on Bio-Oss than observed when osteoblasts were seeded on TCPs,³⁹ and Siggers *et al.* reported lower *ALP*, *OCN*, *BSP*, *RUNX-2*, and *Col I* gene expression in BMSCs seeded on natural bone particles compared with those in BMSCs seeded on TCPs.⁴⁰ Inconsistent co-cultivation models, the use of a variety of chemical agents, and other factors may contribute to the discrepancies in these results.^{11–13,41} Most of these studies were conducted in the presence of chemical osteogenic supplements. From these studies, it is difficult to determine whether xenogenic

FIG. 7. (A) Histological analysis of new bone formation and growth of blood vessels in rabbit mandibles by hematoxylin and eosin (H&E) staining at 4 weeks. (B) Histological analysis of new bone formation and growth of blood vessels in rabbit mandibles by H&E staining at 12 weeks. (C) CD31 staining of the new blood vessels. *Black arrow heads* denote the distribution of the blood vessels. (D) Quantitative analysis of the amount of new bone and bone marrow cavities in H&E staining and blood vessels in CD31 staining. NB, nascent bone; BV, blood vessel. * $p < 0.05$ and ** $p < 0.01$. Color images available online at www.liebertpub.com/tea



bone grafts could promote osteogenic differentiation of MSCs and predict the outcome of their combined use in bone defect repairs. Therefore, to elucidate the capability of promoting osteogenic differentiation of pure grafts, we focused on the cell behavior on the graft material in the absence of osteogenic supplements. In this study, the continuously increased extracellular matrix production and the expression of osteogenic marker gene mRNA in ADSCs seeded in CACB in the absence of osteogenic supplements suggests that CACB alone could initiate the spontaneous differentiation of ADSCs to the osteogenic lineage. The highly branched morphology of the ADSCs suggests that direct cellular tensegrity followed by mechanotransductive events might explain the osteogenic differentiation of ADSCs on CACB. Indirect chemical cues might also be involved. The Ca, P, Si, and Zn ions released from CACB might not only regulate the growth and metabolism of cells but also acti-

vate the expression of related genes to enhance the formation and mineralization of ECMs.^{31–37,42,43}

The temporal kinetics of mRNA expression of osteogenic marker genes in the ADSCs cultured in CACB lagged behind that of ADSCs cultured in OS medium. At day 7, the expression levels of *ALP*, *BMP2*, *BSP*, and *OPN* were higher in the TCPs/OS+ group than those in the CACB/OS– group. Till day 14, the expression levels of the osteogenic marker genes in the CACB/OS– group increased rapidly to reach levels similar to those in the TCPs/OS+ group. At day 21, the expression levels of *OPN* in the CACB/OS– group were much higher than those in the TCPs/OS+ group. This indicates that the chemical bioactive factors were more influential in modulating the cell lineage in the early stage of the experiment, while the biomaterials might provide a suitable temporal signal by the microenvironment of CACB to initiate cell differentiation. The OS medium might induce osteogenic

behavior through a short-cut involving chemical signaling, while the biomaterial niche drove osteogenesis by initiating mechanotransductive mechanisms to activate downstream chemical signaling.⁴⁴⁻⁴⁷ This hypothesis was supported by the continual higher expression levels of the osteogenic marker genes in the CACB/OS+ group, which suggested that the synergistic effects were achieved by the combination of CACB and OS. The ADSCs aggregation observed in the CACB/OS+ group at all experimental time points was probably because these cells were at a more mature differentiation stage. In this study, the early osteogenic-specific cell status of ADSCs might have produced a reduction of cells entering the proliferation cycle, resulting in significant cell proliferation arrest and fewer cell colonization.

The role of the ERK pathway in the osteogenic behavior of ADSCs produced by CACB was explored. ERK1/2, a hub transcription factor in the mechanotransduction mechanism, phosphorylates and activates RUNX-2 during topography-mediated osteogenesis.^{42,43,47,48} The chemical features of Ca^{2+} ,^{42,43} PO_4^{3-} ,⁴³ and Zn^{2+} ,⁴⁹ treatment regulated ERK phosphorylation and influenced the osteogenic differentiation of multipotent cells. We hypothesized that the ERK cascade may serve as a mediator by transducing signals from CACB into cells, thereby regulating the differentiation of ADSCs. Our findings confirmed this hypothesis. CACB initiated a significant increase in the protein levels of P-ERK1/2 and the osteogenic marker RUNX-2. After treatment with the MeK1/2 inhibitor U0126, the attenuated expression of P-ERK1/2 in the ADSCs in CACB was accompanied by an apparent decrease of RUNX-2 expression. A schematic depiction of the involvement of the ERK1/2 signaling pathway in the CACB-mediated osteodifferentiation of RaADSCs is shown in Figure 8. These

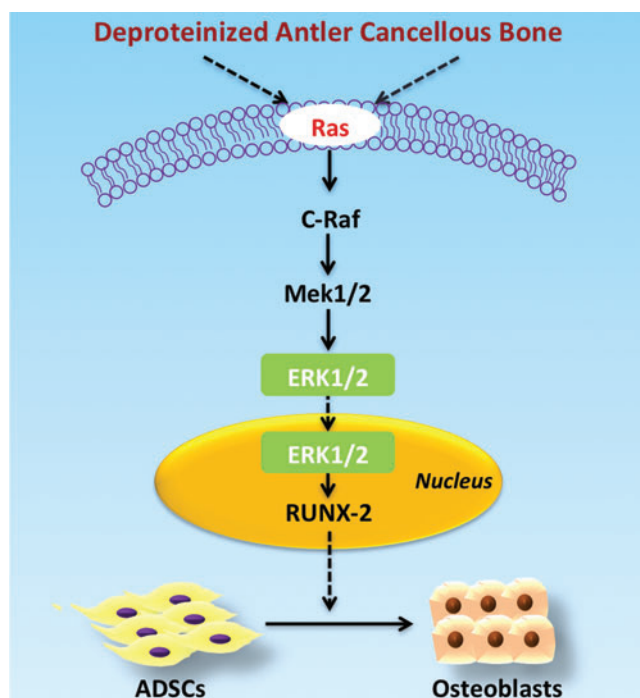


FIG. 8. Schematic depiction of the ERK1/2 signaling pathway and its proposed involvement in the CACB-mediated osteodifferentiation of RaADSCs. Color images available online at www.liebertpub.com/tea

results might be explained by the fact that the enhanced cell adhesion initiated by the CACB topography cues could mediate cytoskeletal reorganization to change the mechanical properties of the cells, which, in turn, activates the downstream mechanotransductive signaling through ERK1/2. In addition, the free ions released by the solid phase of CACB could also activate ERK. These results are consistent with those of previous studies.⁵⁰

This study demonstrated the *in vivo* synergistic effects of ADSCs and CACB to improve bone regeneration. The μ -CT analysis and histological evaluation revealed that loading of ADSCs into CACB increased the quality and quantity of new bone formation. This phenomenon is consistent with the *in vitro* results described earlier, and it is believed that the physicochemical features of CACB (micro- and nano-scale topography, porosity, chemical composition, and ions release) help maintain the bioactivity of ADSCs and spontaneously initiate their osteogenic differentiation. Significantly improved vascularization after implantation of CACB/ADSCs composites was observed. This could be ascribed to the angiogenic effect of ADSCs. ADSCs contribute to vascularization both *in vitro* and *in vivo*, because not only do they differentiate into endothelial cells (ECs) but also they secrete cytokines, including vascular endothelial growth factor, fibroblast growth factor, and hematopoietic growth factor,^{51,52} which are of vital importance to the migration and proliferation of ECs. Vascularization throughout the defect area can not only lead to a better supply of oxygen and nutrients but also secrete BMP2,⁵³ which could, in turn, promote osteogenesis. Thus, the ability of the CACB/ADSCs composites to enhance bone regeneration might be ascribed to the space maintenance of CACB and its complex mimetic microenvironmental cues, which facilitate cell vitality and drive the osteogenic differentiation of ADSCs, and the angiogenic effects of ADSCs.

Conclusion

In this study, the osteogenic behavior of ADSCs produced by CACB and the molecular signaling pathway underlying the effects were investigated. The biomimetic multi-scale topography and chemical niches provided by CACB could promote ADSC viability and favor cell attachment and spreading. Spontaneous osteogenic differentiation of ADSCs was initiated by CACB in a temporal kinetics that lagged behind that induced by OS medium. The ERK signaling pathway could be responsible for the CACB-driven osteogenic behavior of the ADSCs. Synergistic effects of ADSCs and CACB to improve bone regeneration and angiogenesis were achieved in critical-sized rabbit mandibular bone defects. These findings may provide new insights into the regulation of osteogenesis by biomimetic xenografts, thus extending the development of novel bio-scaffolds.

Acknowledgments

The authors acknowledge the National Basic Research Program of China (2012CB933900), the Key International S&T Cooperation Project (2011DFA32190), the National Natural Science Foundation of China (51302005), and the Beijing natural science foundation (7144256, 7144257).

Disclosure Statement

No competing financial interests exist.

References

- Blokhuis, T.J., and Arts, J.J. Bioactive and osteoinductive bone graft substitutes: definitions, facts and myths. *Injury* **42 Suppl 2**, S26, 2011.
- Samartzis, D., Shen, F.H., Goldberg, E.J., and An, H.S. Is autograft the gold standard in achieving radiographic fusion in one-level anterior cervical discectomy and fusion with rigid anterior plate fixation? *Spine (Phila Pa 1976)* **30**, 1756, 2005.
- Farrington, M., Matthews, I., Foreman, J., Richardson, K.M., and Caffrey, E. Microbiological monitoring of bone grafts: two years' experience at a tissue bank. *J Hosp Infect* **38**, 261, 1998.
- Hofmann, C., von Garrel, T., and Gotzen, L. [Bone bank management using a thermal disinfection system (Lobator SD-1). A critical analysis]. *Unfallchirurg* **99**, 498, 1996.
- Marx, R.E. Bone and bone graft healing. *Oral Maxillofac Surg Clin North Am* **19**, 455, 2007.
- Nasr, H.F., Aichelmann-Reidy, M.E., and Yukna, R.A. Bone and bone substitutes. *Periodontol 2000* **19**, 74, 1999.
- Stockmann, P., Park, J., von Wilmsowky, C., Nkenke, E., Felszeghy, E., Dehner, J.F., Schmitt, C., Tudor, C., and Schlegel, K.A. Guided bone regeneration in pig calvarial bone defects using autologous mesenchymal stem/progenitor cells—a comparison of different tissue sources. *J Craniomaxillofac Surg* **40**, 310, 2012.
- Schubert, T., Xhema, D., Veriter, S., Schubert, M., Behets, C., Delloye, C., Gianello, P., and Dufrane, D. The enhanced performance of bone allografts using osteogenic-differentiated adipose-derived mesenchymal stem cells. *Biomaterials* **32**, 8880, 2011.
- Kon, E., Muraglia, A., Corsi, A., Bianco, P., Marcacci, M., Martin, I., Boyde, A., Ruspantini, I., Chistolini, P., Rocca, M., Giardino, R., Cancedda, R., and Quarto, R. Autologous bone marrow stromal cells loaded onto porous hydroxyapatite ceramic accelerate bone repair in critical-size defects of sheep long bones. *J Biomed Mater Res* **49**, 328, 2000.
- Liu, Y., Ming, L., Luo, H., Liu, W., Zhang, Y., Liu, H., and Jin, Y. Integration of a calcined bovine bone and BMSC-sheet 3D scaffold and the promotion of bone regeneration in large defects. *Biomaterials* **34**, 9998, 2013.
- Bareille, R., Lafage-Proust, M.H., Faucheux, C., Laroche, N., Wenz, R., Dard, M., and Amedee, J. Various evaluation techniques of newly formed bone in porous hydroxyapatite loaded with human bone marrow cells implanted in an extra-osseous site. *Biomaterials* **21**, 1345, 2000.
- Gutwald, R., Haberstroh, J., Kuschnierz, J., Kister, C., Lysek, D.A., Maglione, M., Xavier, S.P., Oshima, T., Schmelzeisen, R., and Sauerbier, S. Mesenchymal stem cells and inorganic bovine bone mineral in sinus augmentation: comparison with augmentation by autologous bone in adult sheep. *Br J Oral Maxillofac Surg* **48**, 285, 2010.
- Pieri, F., Lucarelli, E., Corinaldesi, G., Aldini, N.N., Fini, M., Parrilli, A., Dozza, B., Donati, D., and Marchetti, C. Dose-dependent effect of adipose-derived adult stem cells on vertical bone regeneration in rabbit calvarium. *Biomaterials* **31**, 3527, 2010.
- Lu, Z., Roohani-Esfahani, S.I., Wang, G., and Zreiqat, H. Bone biomimetic microenvironment induces osteogenic differentiation of adipose tissue-derived mesenchymal stem cells. *Nanomedicine* **8**, 507, 2012.
- Dawson, J.I., and Oreffo, R.O. Bridging the regeneration gap: stem cells, biomaterials and clinical translation in bone tissue engineering. *Arch Biochem Biophys* **473**, 124, 2008.
- Zhang, X., Cai, Q., Liu, H., Heng, B.C., Peng, H., Song, Y., Yang, Z., and Deng, X. Osteoconductive effectiveness of bone graft derived from antler cancellous bone: an experimental study in the rabbit mandible defect model. *Int J Oral Maxillofac Surg* **41**, 1330, 2012.
- Zhang, X., Xu, M., Song, L., Wei, Y., Lin, Y., Liu, W., Heng, B.C., Peng, H., Wang, Y., and Deng, X. Effects of compatibility of deproteinized antler cancellous bone with various bioactive factors on their osteogenic potential. *Biomaterials* **34**, 9103, 2013.
- Gimble, J.M., Katz, A.J., and Bunnell, B.A. Adipose-derived stem cells for regenerative medicine. *Circ Res* **100**, 1249, 2007.
- Sakaguchi, Y., Sekiya, I., Yagishita, K., and Muneta, T. Comparison of human stem cells derived from various mesenchymal tissues: superiority of synovium as a cell source. *Arthritis Rheum* **52**, 2521, 2005.
- Mizuno, H., Tobita, M., and Uysal, A.C. Concise review: adipose-derived stem cells as a novel tool for future regenerative medicine. *Stem Cells* **30**, 804, 2012.
- Cui, L., Liu, B., Liu, G., Zhang, W., Cen, L., Sun, J., Yin, S., Liu, W., and Cao, Y. Repair of cranial bone defects with adipose derived stem cells and coral scaffold in a canine model. *Biomaterials* **28**, 5477, 2007.
- Lendeckel, S., Jodicke, A., Christophis, P., Heidinger, K., Wolff, J., Fraser, J.K., Hedrick, M.H., Berthold, L., and Howaldt, H.P. Autologous stem cells (adipose) and fibrin glue used to treat widespread traumatic calvarial defects: case report. *J Craniomaxillofac Surgery* **32**, 370, 2004.
- Mesimaki, K., Lindroos, B., Tornwall, J., Mauno, J., Lindqvist, C., Kontio, R., Miettinen, S., and Suuronen, R. Novel maxillary reconstruction with ectopic bone formation by GMP adipose stem cells. *Int J Oral Maxillofac Surg* **38**, 201, 2009.
- Thesleff, T., Lehtimäki, K., Niskakangas, T., Mannerstrom, B., Miettinen, S., Suuronen, R., and Ohman, J. Cranioplasty with adipose-derived stem cells and biomaterial: a novel method for cranial reconstruction. *Neurosurgery* **68**, 1535, 2011.
- Syed-Picard, F.N., Jayaraman, T., Lam, R.S., Beniash, E., and Sfeir, C. Osteoinductivity of calcium phosphate mediated by connexin 43. *Biomaterials* **34**, 3763, 2013.
- Muller, P., Bulnheim, U., Diener, A., Luthen, F., Teller, M., Klinkenberg, E.D., Neumann, H.G., Nebe, B., Liebold, A., Steinhoff, G., and Rychly, J. Calcium phosphate surfaces promote osteogenic differentiation of mesenchymal stem cells. *J Cell Mol Med* **12**, 281, 2008.
- Li, X., Liu, H., Niu, X., Fan, Y., Feng, Q., Cui, F.Z., and Watari, F. Osteogenic differentiation of human adipose-derived stem cells induced by osteoinductive calcium phosphate ceramics. *J Biomed Mater Res B Appl Biomater* **97**, 10, 2011.
- Sun, J.S., Chang, W.H., Chen, L.T., Huang, Y.C., Juang, L.W., and Lin, F.H. The influence on gene-expression profiling of osteoblasts behavior following treatment with the ionic products of sintered beta-dicalcium pyrophosphate dissolution. *Biomaterials* **25**, 607, 2004.
- Gorbunoff, M.J., and Timasheff, S.N. The interaction of proteins with hydroxyapatite. III. Mechanism. *Anal Biochem* **136**, 440, 1984.
- Gilbert, M., Shaw, W.J., Long, J.R., Nelson, K., Drobny, G.P., Giachelli, C.M., and Stayton, P.S. Chimeric peptides

- of statherin and osteopontin that bind hydroxyapatite and mediate cell adhesion. *J Biol Chem* **275**, 16213, 2000.
31. Sun, H., Wu, C., Dai, K., Chang, J., and Tang, T. Proliferation and osteoblastic differentiation of human bone marrow-derived stromal cells on akermanite-bioactive ceramics. *Biomaterials* **27**, 5651, 2006.
 32. Hussain, A., Bessho, K., Takahashi, K., and Tabata, Y. Magnesium calcium phosphate as a novel component enhances mechanical/physical properties of gelatin scaffold and osteogenic differentiation of bone marrow mesenchymal stem cells. *Tissue Eng Part A* **18**, 768, 2012.
 33. Amaral, M., Costa, M.A., Lopes, M.A., Silva, R.F., Santos, J.D., and Fernandes, M.H. Si(3)N(4)-bioglass composites stimulate the proliferation of MG63 osteoblast-like cells and support the osteogenic differentiation of human bone marrow cells. *Biomaterials* **23**, 4897, 2002.
 34. Nair, M.B., Bernhardt, A., Lode, A., Heinemann, C., Thieme, S., Hanke, T., Varma, H., Gelinsky, M., and John, A. A bioactive triphasic ceramic-coated hydroxyapatite promotes proliferation and osteogenic differentiation of human bone marrow stromal cells. *J Biomed Mater Res A* **90**, 533, 2009.
 35. Honda, M., Kikushima, K., Kawanobe, Y., Konishi, T., Mizumoto, M., and Aizawa, M. Enhanced early osteogenic differentiation by silicon-substituted hydroxyapatite ceramics fabricated via ultrasonic spray pyrolysis route. *J Mater Sci Mater Med* **23**, 2923, 2012.
 36. Luo, X., Barbieri, D., Davison, N., Yan, Y., de Bruijn, J.D., and Yuan, H. Zinc in calcium phosphate mediates bone induction: *in vitro* and *in vivo* model. *Acta Biomater* **10**, 477, 2014.
 37. Oh, S.A., Kim, S.H., Won, J.E., Kim, J.J., Shin, U.S., and Kim, H.W. Effects on growth and osteogenic differentiation of mesenchymal stem cells by the zinc-added sol-gel bioactive glass granules. *J Tissue Eng* **2010**, 475260, 2011.
 38. Acil, Y., Terheyden, H., Dunsche, A., Fleiner, B., and Jepsen, S. Three-dimensional cultivation of human osteoblast-like cells on highly porous natural bone mineral. *J Biomed Mater Res* **51**, 703, 2000.
 39. Kubler, A., Neugebauer, J., Oh, J.H., Scheer, M., and Zoller, J.E. Growth and proliferation of human osteoblasts on different bone graft substitutes: an *in vitro* study. *Implant Dent* **13**, 171, 2004.
 40. Siggers, K., Frei, H., Fernlund, G., and Rossi, F. Effect of bone graft substitute on marrow stromal cell proliferation and differentiation. *J Biomed Mater Res A* **94**, 877, 2010.
 41. Sadeghi, D., Nazarian, H., and Nojehdehian, H. Adipose-derived stem cells combined with beta-tricalcium phosphate: a novel possible strategy for periodontal defects regeneration. *Med Hypotheses* **82**, 54, 2014.
 42. Barradas, A.M., Fernandes, H.A., Groen, N., Chai, Y.C., Schrooten, J., van de Peppel, J., van Leeuwen, J.P., van Blitterswijk, C.A., and de Boer, J. A calcium-induced signaling cascade leading to osteogenic differentiation of human bone marrow-derived mesenchymal stromal cells. *Biomaterials* **33**, 3205, 2012.
 43. Khoshniat, S., Bourguine, A., Julien, M., Petit, M., Pilet, P., Rouillon, T., Masson, M., Gatius, M., Weiss, P., Guicheux, J., and Beck, L. Phosphate-dependent stimulation of MGP and OPN expression in osteoblasts via the ERK1/2 pathway is modulated by calcium. *Bone* **48**, 894, 2011.
 44. Igarashi, M., Kamiya, N., Hasegawa, M., Kasuya, T., Takahashi, T., and Takagi, M. Inductive effects of dexamethasone on the gene expression of Cbfa1, Osterix and bone matrix proteins during differentiation of cultured primary rat osteoblasts. *J Mol Histol* **35**, 3, 2004.
 45. Mikami, Y., Omoteyama, K., Kato, S., and Takagi, M. Inductive effects of dexamethasone on the mineralization and the osteoblastic gene expressions in mature osteoblast-like ROS17/2.8 cells. *Biochem Biophys Res Commun* **362**, 368, 2007.
 46. Ito, S., Suzuki, N., Kato, S., Takahashi, T., and Takagi, M. Glucocorticoids induce the differentiation of a mesenchymal progenitor cell line, ROB-C26 into adipocytes and osteoblasts, but fail to induce terminal osteoblast differentiation. *Bone* **40**, 84, 2007.
 47. Wang, C., Lin, K., Chang, J., and Sun, J. Osteogenesis and angiogenesis induced by porous beta-CaSiO(3)/PDLGA composite scaffold via activation of AMPK/ERK1/2 and PI3K/Akt pathways. *Biomaterials* **34**, 64, 2013.
 48. Gu, H., Guo, F., Zhou, X., Gong, L., Zhang, Y., Zhai, W., Chen, L., Cen, L., Yin, S., Chang, J., and Cui, L. The stimulation of osteogenic differentiation of human adipose-derived stem cells by ionic products from akermanite dissolution via activation of the ERK pathway. *Biomaterials* **32**, 7023, 2011.
 49. Liu, Y., Yan, F., Yang, W.L., Lu, X.F., and Wang, W.B. Effects of zinc transporter on differentiation of bone marrow mesenchymal stem cells to osteoblasts. *Biol Trace Elem Res* **154**, 234, 2013.
 50. Zhang, H., Liu, S., Zhou, Y., Tan, J., Che, H., Ning, F., Zhang, X., Xun, W., Huo, N., Tang, L., Deng, Z., and Jin, Y. Natural mineralized scaffolds promote the dentinogenic potential of dental pulp stem cells via the mitogen-activated protein kinase signaling pathway. *Tissue Eng Part A* **18**, 677, 2012.
 51. Kilroy, G.E., Foster, S.J., Wu, X., Ruiz, J., Sherwood, S., Heifetz, A., Ludlow, J.W., Stricker, D.M., Potiny, S., Green, P., Halvorsen, Y.D., Cheatham, B., Storms, R.W., and Gimble, J.M. Cytokine profile of human adipose-derived stem cells: expression of angiogenic, hematopoietic, and pro-inflammatory factors. *J Cell Physiol* **212**, 702, 2007.
 52. Kim, K.I., Park, S., and Im, G.I. Osteogenic differentiation and angiogenesis with cocultured adipose-derived stromal cells and bone marrow stromal cells. *Biomaterials* **35**, 4792, 2014.
 53. Li, H., Xue, K., Kong, N., Liu, K., and Chang, J. Silicate bioceramics enhanced vascularization and osteogenesis through stimulating interactions between endothelial cells and bone marrow stromal cells. *Biomaterials* **35**, 3803, 2014.

Address correspondence to:

Xuliang Deng, MD, PhD

Department of Geriatric Dentistry

National Engineering Laboratory for Digital and Material

Technology of Stomatology

Peking University School and Hospital of Stomatology

Beijing 100081

People's Republic of China

E-mail: kqdengxuliang@bjmu.edu.cn

Yan Wei, MD, PhD

Department of Geriatric Dentistry

Peking University School and Hospital of Stomatology

Beijing 100081

People's Republic of China

E-mail: kqweiyang@126.com

Received: July 4, 2014

Accepted: February 23, 2015

Online Publication Date: April 10, 2015